IL NUOVO CIMENTO Vol. 30 C, N. 5 Settembre-Ottobre 2007
DOI 10.1393/ncc/i2008-10263-y

SiPM: Characterizations, modelling and VLSI front-end dedicated development(*)

D. Badoni(1)(2), R. Messi(1)(2), V. Bidoli(2), V. Capuano(2), M. Casolino(1)(2), P. Picozza(1)(2) and A. Popov(3)

(1) *INFN Sezione di Roma "Tor Vergata" - Rome, Italy*
(2) *Dipartimento di Fisica, Università di Roma "Tor Vergata" - Rome, Italy*
(3) *MEPHI - Moscow, Russia*

(ricevuto il 3 Marzo 2008; pubblicato online il 28 Aprile 2008)

Summary. — In this work we describe the results of performance tests and measures of SiPM of several sizes (1×1, 3×3, 5×5) delivered from MEPHI. The SiPMs have been studied both in steady and pulsed stimuli. Aging and temperature behavior are also discussed. Another test has been performed in order to obtain an electrical model of the SiPM to be used in analog simulations. Finally, a design of a pilot chip with 0.35 μm technology implementing a front-end for SiPM aimed to TOF applications with adjustable thresholds and very high dynamical range is described.

PACS 07.87.+v – Spaceborne and space research instruments, apparatus, and components (satellites, space vehicles, etc.).
PACS 95.55.Aq – Charge-coupled devices, image detectors, and IR detector arrays.
PACS 85.30.De – Semiconductor-device characterization, design, and modeling.
PACS 85.40.-e – Microelectronics: LSI, VLSI, ULSI; integrated circuit fabrication technology.

1. – Introduction

In this paper we present the Silicon Photomultiplier (SiPM) characteristic, studied in both steady state and pulsed modes. We report also the study of a full custom Front End (FE) chip developed by INFN - Sez. Roma "Tor Vergata" in the framework of the Wizard Collaboration. Furthermore we have studied the possibility to realize a TOF detector in space-based experiments taking into account power, mass and radiation resistance constraints. The SiPM is a good candidate detector for its fast response, good quantum efficiency, dimension and power consumption. We have studied three different diodes

(*) Paper presented at the 1st Workshop on Photon Detection for High Energy Medical and Space Applications; Perugia, June 13-14, 2007.

produced by MEPHI group (1×1, 3×3 and $5 \times 5\,\mathrm{mm}^2$) [1, 2]. The first and third types have been used to study the coupling SiPM-scintillator problems like efficiency, time response and different coupling topology. The $3 \times 3\,\mathrm{mm}^2$ has good linearity response due to high pixel number and has therefore been used to determine the characteristic curves both in steady-state current and in pulsed mode as a function of temperature and integrated charges (aging). Our data set is obtained using two diodes 5×5, six diodes 3×3 and four 1×1 SiPM. Furthermore we present the measures on the SiPM for modelling its electrical properties. This model has been used for the analog simulation of the analog VLSI front-end. We discuss this analog VLSI implementation of a prototype chip with eight channels aimed to TOF application with independent adjustable thresholds and wide dynamical range.

2. – Steady condition characteristics

We have studied the reduced gain *R. Gain* as a function of the working temperature and integrated charge. The usual definition of the gain is $G = \frac{(V_b - V_{BD})\, C_D}{q}$ (where V_b is the bias voltage and V_{BD} the breakdown voltage), it contains the diode equivalent capacitance C_d and the initial charge q which is a function of the number of fired pixels. The C_d parameter is measured by the technique described below. In order to measure the initial charge q we have to know the number of the incoming photons to the SiPM detector. Since we are interested to study the relative values of the gain we have used the following definition: $R.Gain = \frac{I_{\mathrm{out}}}{I_{\mathrm{in}}}$ normally used for the APD [3] where I_{in} and I_{out} are, respectively, the current values for unitary gain ($V_b \ll V_{BD}$) and for gain equal to *R. Gain* (V_b close V_{BD}). The I_{in} and I_{out} were also corrected for the dark current: $I_{\mathrm{in}} = I_{\mathrm{inlight}} - I_{\mathrm{indark}}$ and $I_{\mathrm{out}} = I_{\mathrm{outlight}} - I_{\mathrm{outdark}}$. This definition is valid only for gains lower than 300–500, but is not valid for values above this limit where it is not possible to define I_{in} correctly. In our case the I_{in} was defined by the condition $V_b \ll V_{BD}$ where all the characteristic curves (about 80) were linear and constant.

3. – Gain as a function of temperature

We have used a small cold-finger liquid-nitrogen cryostat at variable temperature. The SiPM detector was glued by silver-paint in the cold finger in order to have good thermal contact. The cold-finger temperature was monitored by a platinum thermometer, while the SiPM temperature was monitored by a silicon (Cryophysics DT470) thermometer glued very close to detector. All the apparatus was illustrated in fig. 1.

In fig. 2 14 dark current curves *I-V* are illustrated as a function of temperature ranging between 129 K and 300 K. Two important points should be noticed: the first one is the decrease of V_{BD} in accordance to the temperature decrease; the second one is that below 230 K the curves show a point of inflection, while above 230 K they show a quadratic behavior. It should be also noticed that the leakage current increases very fast for $T > 273$ K. This is very important for future experimental application. Similar behavior is visible in fig. 3 where the reduced gain is shown.

Comparing the last two plots it is obvious that the reduced gain is an approximated definition. In fig. 4 the reduced gain is shown as a function of temperature (at fixed V_b). As shown, starting from 300 K, the gain increases as the temperature decreases: this is due both to recombination process and free charges available. It is important to notice that is not useful to choose a working point below 260 K, obtained with a Peltier Cell or a CO_2 cooling system. Future investigation below 260 K should be done.

Fig. 1. – Cold-finger liquid-nitrogen cryostat and SiPM-thermometer glued.

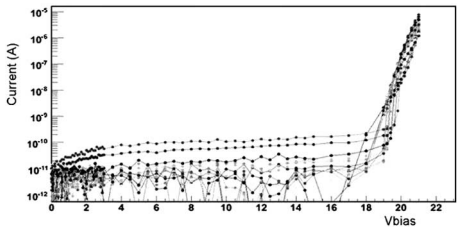

Fig. 2. – Dark current *vs.* V_b as a function of temperature.

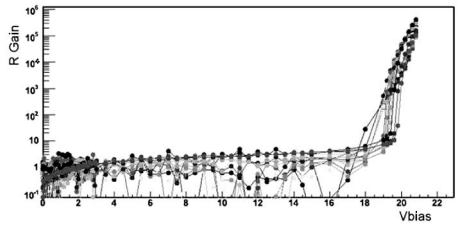

Fig. 3. – Dark *R. Gain vs.* V_b as a function of temperature.

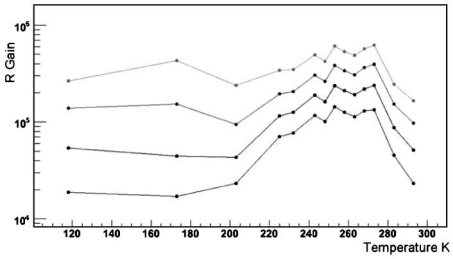

Fig. 4. – Last four highest *R. Gain* points for the curve in fig. 3 as a function of temperature.

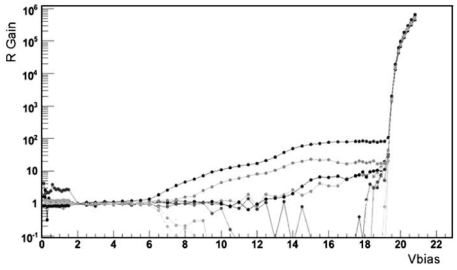

Fig. 5. – Behavior of the *R. Gain vs.* V_b curves as a function of integrated charge from zero to 0.8 mC.

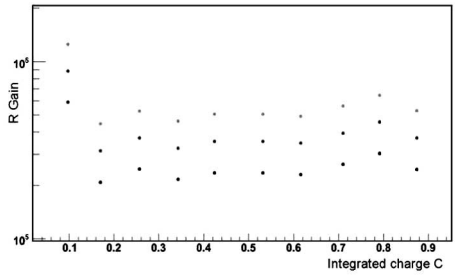

Fig. 6. – Last four highest *R. Gain* points for the curve in fig. 5 as a function of integrated charge.

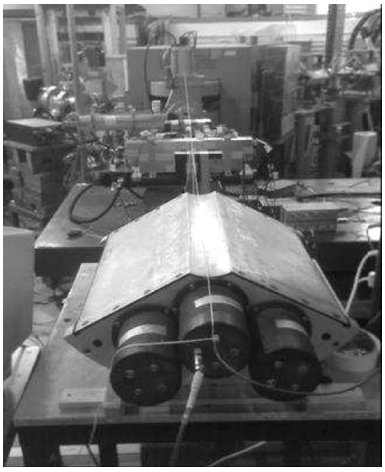

Fig. 7. – Experimental apparatus at BTF electron facility at LNF.

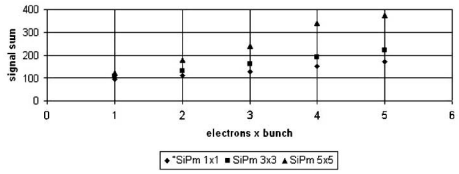

Fig. 8. – Dependence on delivery light detected.

4. – Aging measurement

The aim of this measure should be to investigate the behavior of the aging process as a function of the integrated charge. We have used three diodes 3×3 in order to have a statistical significance. The experimental apparatus consists of a led in front of the three SiPMs, we choose a working point where the SiPM integrates 80 mC/20 min, and the SiPM works in the linear region. The polarization of the SiPM is obtained by programmable Keithley 2410 power supply and the current was monitored by a Keithley 6514 picoamperometer connected to the computer system. For any point of integrated charge two curves I–V were measured in dark and light conditions in order to calculate the reduced gain (*R. Gain*). All this measure was done at constant temperature of 22 °C. The total integrated charge was about 0.9 C. In fig. 5 the reduced gain as a function of the V_b for different integrated charges is shown. It is important to notice that the V_{BD} remains constant while the leakage increases, that means the intrinsic noise also increases. In fig. 6 the reduced gain as a function of the integrated charge (for three different values of V_b) is shown: the gain remains constant up to about 1 C. The first experimental point was made in different conditions.

5. – Pulsed measure

In this case we have used the BTF at LNF, Frascati. We have used the three different available diodes in different topological coupling to BC408 scintillator (blue-light emission around 400 nm). In fig. 7 the experimental apparatus is shown where the electromagnetic calorimeter providing the number of electrons in any bunch is visible. Our apparatus is visible in the center of the system together with the trigger system and the beam pipe. The SiPM 1×1 was coupled with the scintillator ($30 \times 30\,\mathrm{mm}^2$) through a wavelength shifter fiber (WLS Y11). These detectors were produced in the middle of 2004. The other SiPM (type 3×3 and $5 \times 5\,\mathrm{mm}^2$) was glued close to the diametrically opposed corner of scintillator square slide ($75 \times 75 \times 5\,\mathrm{mm}^3$). The linearity response of the detectors was

TABLE I. – *Amplitude of two diametrically opposite SiPM functions of different zones fired.*

y \ x	-30	0	$+30$
$+12$	119.1	123.6	120.4
0	120.6	124.6	120.3
-12			118.0

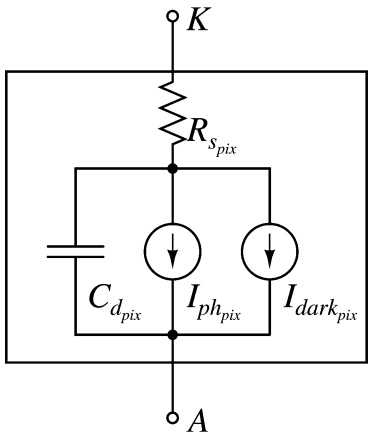

Fig. 9. – Equivalent circuit for the single pixel.

fine for low signal, we present the results for all types of SiPM for a maximum number of 5 incident electrons on the scintillator (see fig. 8). We have a good uniform response *vs.* a different area fired from the electron bunch: in table I we show the sum of the analogical amplitude of two diametrically opposite SiPM functions of different zones fired.

6. – SiPM model

Although SiPM has been available for many years, the analog electronics for optimization of some of its performance is still currently under study. A good model useful for a typical analog simulation in a VLSI project framework has been developed. This model takes into account the specific architecture of the SiPM consisting of several *pixels* connected in parallel all together. We have used a simplified model of the SiPM in order to obtain a faster simulation without degrading the reliability: in the architecture some elements are omitted, and the second-order effects as after-pulsing or optical cross-talk are not modelled.

The first step for modelling is designing an equivalent circuit for the single pixels connected all together in parallel as shown in fig. 9. The $I_{\mathrm{dark_{pix}}}$ takes into account the thermal current, it depends on temperature and bias voltage V_b and represents the time integral mean of the current. The $C_{d_{\mathrm{pix}}}$ is the junction capacitance, it depends on V_b and on the depth of the depletion layer. The $R_{s_{\mathrm{pix}}}$ is the ohmic resistor for the geiger mode current limitation. The $I_{ph_{\mathrm{pix}}}$ is a current generator; it takes into account the incoming photon(s): the time waveform is square and the time width has been fixed very short.

The constant recovery time of the single pixel depends on C_{pix} and the series resistor composed by $R_{s_{\mathrm{pix}}}$ plus the external loading resistor.

The choice of different amplitudes I allows to emulate the corresponding charge production: $Q(t) = I \cdot T$ which corresponds to different SiPM gains.

The parameters of the equivalent circuit have been derived from measures on the SiPM.

We assumed that parameters in all pixels are the same and that the array is equivalent to a circuit with the same architecture and parameters linearly scaled as shown in fig. 10. The event of n incoming photons which simultaneously arrives at different pixels can be obtained by multiplying the generated current for n: $I_{\mathrm{ph}}(n) = I_{\mathrm{ph}} \cdot n$.

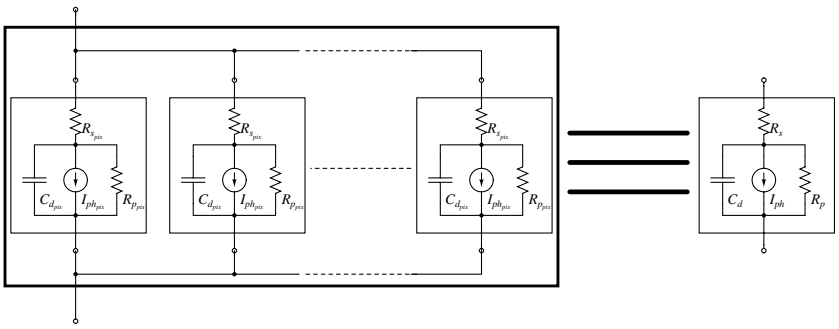

Fig. 10. – Equivalent circuit for the global model. With the approximation that parameters of all pixels are the same, the single-pixel parameters (with *pix*) extension on the left side of the figure have a linear relationship with the parameters in the global representation on the right side of the figure.

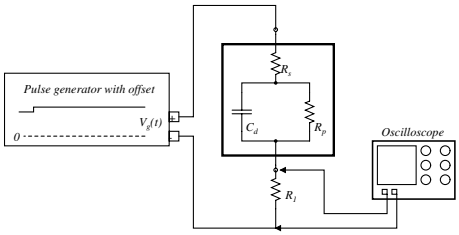

Fig. 11. – Experimental set-up for the measures of the global parameter.

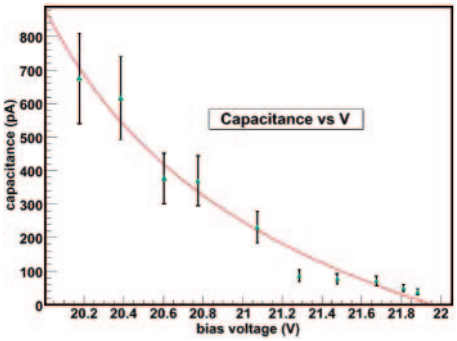

Fig. 12. – Relationship between the depletion capacitance and bias voltage V_b applied.

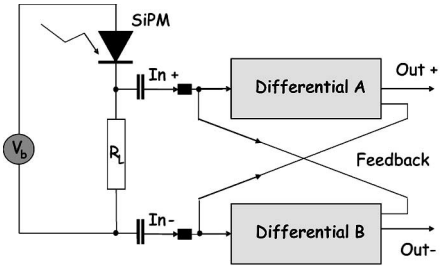

Fig. 13. – Fully differential current amplifier. Topological scheme.

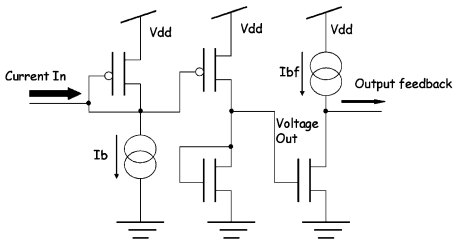

Fig. 14. – One side (A or B) of fully differential current amplifier: simplified schematic of *fully balanced* current amplifier.

The equivalent circuit composed of the arrays of single pixels can be used in simulation with the advantage of making it possible to reproduce a flow of incoming photons which arrives in a certain time; the disadvantage is that the simulation may be run slowly due to a typical high number of pixels in array (*i.e.* 5625 in our used model).

The global equivalent circuit represented on the right side of fig. 10 can be advantageously used in the simulation without substantially affecting the performance of the simulation. The potential disadvantage is that is not possible to consider a flow of n incoming photons arriving in a time comparable with the constant recovery time of the SiPM; the time width must be: or very short, in this case we use $I_{\mathrm{ph}}(n)$ as mentioned before; or the time between two incoming photons (or group) must be greater than the constant recovery time of the SiPM. We use the last choice for the development of front-end electronics since the project is oriented to a TOF application in space-born experiments where the rate of events may be quite slow and the incoming photons relative to a single event can be considered simultaneous.

6˙1. *Procedure of the measures on SiPM for modelling.* – The parameter of the global model has been obtained through the experimental set-up shown in fig. 11.

All measures have been performed in dark-light condition, so the dark current generator has not been considered. A low step voltage superimposed at the bias voltage has been applied to the SiPM. Through the oscilloscope the constant time has been measured; finally knowing the values of the series resistors, the value of the capacitance has been carried out. The measures have been repeated for several values of V_b. Figure 12

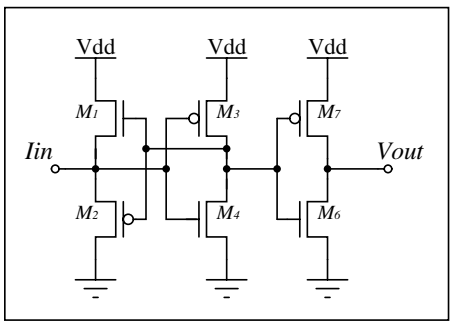

Fig. 15. – Fast current comparator.

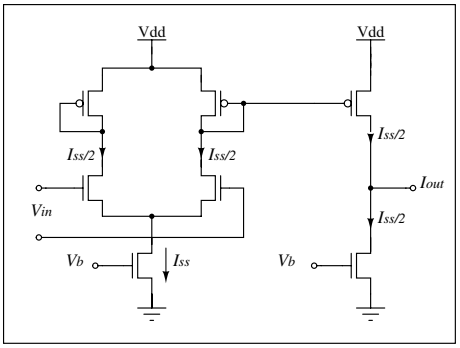

Fig. 16. – Coupling circuit. This circuit transforms the output of preamplifier from differential to single-ended.

shows the relationship between capacitance and V_b. The measures fit well the relationship $C_d \approx \frac{1}{\sqrt{V_b}}$ as expected.

An important parameter of the SiPM is the linearity: the amplitude of the signal *vs.* the number n of the pixels stroked from simultaneous incoming photons. Named M the numbers of pixels of the array always is: maximum $n < M$. In the present work we have considered the data provided by MEPHI: for the 3×3 SiPM with $M = 5625$ the range of linearity is nearly 1–1000. We have fixed also the gain of SiPM at $400000\, e^-$.

7. – An analog VLSI front-end

This design has been developed with $0.35\,\mu$ CMOS AMS technology, with four metals, two polysilicon layers, a high-resistivity layer.

It is intended for using in detecting time where the rates of the events are not high, in particular where the time between events is less than the time constant of the SiPM with its front-end. In such condition each event produces a current pulse where the height is proportional to the number of simultaneous incoming photons which is, finally, proportional to the Z^2 of the particle detected in the scintillator. Thus, we have developed an electronics with a large dynamical range and with a fast response of the front-end. This *double side* of this functionality permits to obtain a trigger from the event and a sort

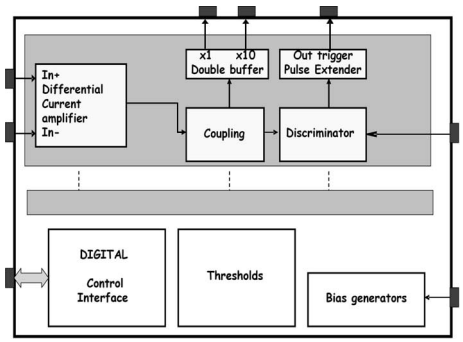

Fig. 17. – General architecture of the proposed chip.

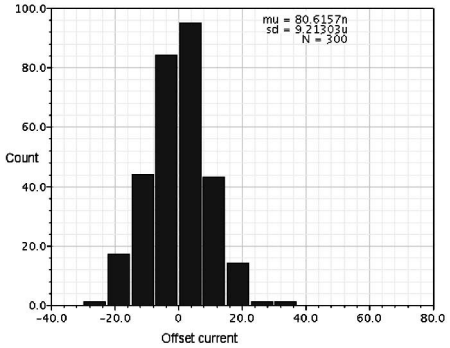

Fig. 18. – Monte Carlo simulation: offset current distribution.

of *masking* for particles with a $Z < Z_{\mathrm{thr}}$, where Z_{thr} is the minimum Z for producing a pulse. The threshold for Z is adjustable in a large dynamical range.

Once the loading impedance of the input preamplifier has been defined (which determines also the constant recovery time of SiPM), the peak value of the pulse generated from the SiPM for 1 pixel is also fixed.

With this scenario we choose the approach of *Current amplifier* for front-end since we would like a high dynamical range: namely 1–1000 and a faster rise-time in input to the discriminator. These requirements are hard to satisfy with conventional voltage amplifiers. Also the recovery time of the complete system (SiPM with front-end) has to be kept at the minimum: this implies a minimum dynamical series impedance at the SIPM. This requirement to match very well with the general low input impedance of a current amplifier.

The chip designed has to be considered as *pilot prototype chip* needed for testing the *proposed analog circuits*.

We illustrate below the main significant circuit of the FE.

In fig. 13 the topological scheme of the preamplifier stage with its connections to the SiPM is shown. The choice of fully differential configuration assures a good immunity at the common-mode noise. Furthermore this configuration permits to introduce a current feedback which improves twice the bandwidth ($\times 2$) and the input impedance ($\times 1/2$).

In fig. 14 the simplified schematic of one preamplifier is shown. The current generators I_b and I_{bf} set the quiescent point of the preamplifier. The input current coming in the p-mos in the branch on the left side is mirrored in the middle branch where a voltage

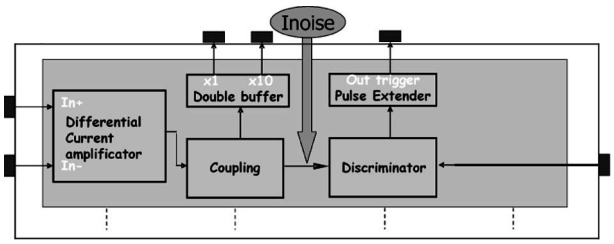

Fig. 19. – Intrinsic jitter estimation.

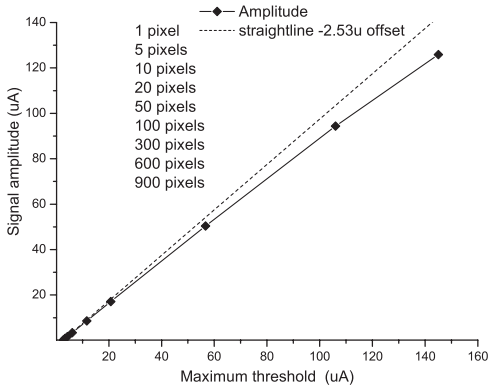

Fig. 20. – Linearity: the simulated point and the nearest straight line with the same offset of $-2.53\,\mu$A.

signal is available, also this signal drives the right branch where the feed-back current is generated. The *fully-balanced* feature is used to reduce the offset current in the output of the stage. This architecture is suitable for low-voltage applications and reduces the mismatch effects of the mosfets [4-6].

Another fundamental module is the discriminator: a fast current comparator [7]. As in the preamplifier, the current domain assures excellent performances in terms of speed and large dynamical range, which cannot be obtained with the corresponding voltage comparators. In fig. 15 the simplified schematic of the current comparator is shown. It is substantially a fast zero crossing. It works well both for low and high currents. An improved version of this comparator described in detail in [8] has been used. Since the discriminator is a single-ended zero-crossing, we need to place a circuit between the preamplifier and the comparator to transform the differential output to a single-ended output. This solution does not degrade the features with respect to external common-mode noise immunity, and introduces only a very little sensitivity at the internal common-mode noise. Figure 16 shows the circuit. It is composed of two stages: a simple differential pair and a current mirror.

7˙1. *General architecture of the chip.* – The general architecture of the prototype chip is shown in fig. 17. It consists of eight channels. Each channel includes the *fully-differential current amplifier*, a *coupling circuit*, a *discriminator* (current-comparator), a *pulse-extender* module and two analog buffers (one of this amplifies ten times than the other one) in order to view the pulses on an oscilloscope. The *pulse extender* is a module which stretches out the time width of the output when it is too short: this happens in particular conditions when the amplitude of SiPM signal is near to the threshold. The *bias generator* is the module which generates the reference currents for all internal current generators.

The current thresholds are independent of each channel.

8. – Results of simulations: performance

The above-described circuit has been tested with typical, corners and Monte Carlo analog simulations. The parameters under test are: 1) dynamical range of thresholds;

2) rise time in the input of comparator; 3) power consumption; 4) threshold offset; 5) estimation of the jitter; 6) linearity.

Concerning the dynamical range of thresholds we obtain 160 μA for a maximum of 1000 equivalent pixels, adjustable at the step of 1 pixel and with a minimum value of 3 pixels. The rise rime is about 2 ns and the power consumption is 16 mW/channel. The thresholds offset is shown in fig. 18 as a result of a *Monte Carlo simulation*, which provides an estimation on the offset current distribution on several channels on the same chip. Although the sigma is 9 μA this is an acceptable value since a threshold is independently adjustable for each channel. The *corner simulation* shows a maximum of -5–$+15$ μA of current thresholds offset over all conditions simulated.

Concerning the jitter estimation we have considered the effect of intrinsic noise (coming from internal mosfet and resistor) as shown in fig. 19. A spectral analysis has been performed: the total equivalent noise has been calculated on the input comparator node. We have used this value inserting as a current constant perturbation. The result for the jitter is J_{int} is: $20 < J_{\text{int}} < 50$ (ps).

The linearity, intended as maximum threshold *vs.* amplitude of the signal, is good and shown in fig. 20.

9. – Conclusion

We have studied the temperature characteristics and the beam test response of SiPMs of various sizs. We have investigated the behavior of the aging process as a function of the integrated charge: an important resulting aspect is that the gain remains constant up to about 1 C of the integrated charge. The behavior of the characteristics of the diodes as a function of the temperature ranging between 129 K and 300 K was investigated. We present the new behavior for a temperature range from 118 K to 300 K. The leakage current increases very fast for $T > 273$ K and below 230 K: the curves show an anomalous behavior. The test to the BTF in LNF at Frascati shows a good linearity and uniform response *vs.* different areas fired of different coupled SiPM-Scintillator types. Furthermore we have designed and simulated with success a chip with 8 channels of front-end for SiPM, aimed to TOF applications with independent adjustable thresholds and large dynamical range; the chip was submitted in September 2007 for production. It was delivered last January 2008 and now is currently under test. This test permits to adjust and consolidate the choice for the circuits.

REFERENCES

[1] Bondarenko G. and Dolgshein B., *Nucl. Phys. B*, **61** (1998) 347.
[2] Buzhan P. and Dolgshein B., *Nucl. Instrum. Methods. A*, **504** (2003) 48.
[3] Karar A., Musienko Y. and Vanel J. Ch., *Nucl. Instrum. Methods. A*, **428** (1999) 413.
[4] Sun B. and Yuan F., *Circuits and Systems, MWSCAS-2002*, **2** (2002) 57.
[5] Sun B. and Yuan F., *A new differential CMOS current pre-amplifier for optical communication*, in *Proceedings of IEEE ISCAS'03*, Vol. **1** (May 2003), pp. 341–344.
[6] Sun B., Yuan F. and Opal A., *Analog Integrated Circuits and Signal Processing*, **44** (2005) 191.
[7] Traff H., *Electron. Lett.*, **28** (1992) 310.
[8] Lin H., Huang J. H. and Wong S. C., *A simple high-speed low current comparator*, in *IEEE International Symposium on Circuit and System, 2000*, ISCAS 2000 Geneva.